Applied Catalysis A: General 462–463 (2013) 278–286

Contents lists available at SciVerse ScienceDirect

Applied Catalysis A: General

journal homepage: www.elsevier.com/locate/apcata

Novel catalyst for the WGS reaction in a Pd-membrane reactor

Carolina A. Cornaglia[a], Silvano Tosti[b], Mirko Sansovini[b], John Múnera[a], Eduardo A. Lombardo[a,*]

[a] Instituto de Investigaciones en Catálisis y Petroquímica (FIQ, UNL-CONICET), Santiago del Estero 2829, 3000 Santa Fe, Argentina
[b] ENEA, Unità Tecnica Fusione, C.R. ENEA Frascati, Via E. Fermi 45, 00044 Frascati, RM, Italy

ARTICLE INFO

Article history:
Received 26 December 2012
Received in revised form 11 April 2013
Accepted 13 April 2013
Available online xxx

Keywords:
Pt catalyst
Stability
CH_4 selectivity
H_2 production
H_2 purification

ABSTRACT

A $Pt/La_2O_3{\cdot}SiO_2$ catalyst was synthesized and tested in the WGS reaction. Kinetic measurements were carried out in a conventional fixed-bed reactor operated in differential mode while the stability test was conducted in integral regime. The fresh and used catalysts were characterized through XRD, XPS, Raman spectroscopy and H_2 chemisorption. The Pt(0.6 wt%)/La_2O_3(27 wt%)·SiO_2 catalyst showed high activity and WGS selectivity, no carbon formation and high stability. After use no changes were observed in the Pt dispersion. The catalyst was also tested in a tubular Pd-Ag membrane reactor in order to gauge the performance of this device using CO conversion, hydrogen recovery and H_2 production as parameters. The membrane reactor experiments were performed between 673 and 723 K and at pressures ranging from 100 kPa to 800 kPa. The low methanation activity was monitored in all cases. Under the best operating conditions, a CO conversion of 98% and a hydrogen recovery of 90% were reached operating at 800 kPa in the retentate side, and at 100 kPa in the permeate side.

© 2013 Elsevier B.V. All rights reserved.

1. Introduction

The use of the hydrogen as a "clean" energy vector can mitigate both greenhouse gas emissions and related climate changes, particularly when it is produced from renewable sources [1–3]. The combustion of hydrogen produces water with no environmental impact.

Presently, hydrogen is produced mainly via the reforming of hydrocarbons [4,5]. The water gas shift (WGS) reaction is an important step in the purification of the reformed stream to obtain hydrogen with a low CO content.

$$CO + H_2O \leftrightarrow CO_2 + H_2 \Delta h^\circ = -41\ \mathrm{kJ\,mol^{-1}}$$

For instance, for feeding PEM fuel cells ultra-pure hydrogen is required because the Pt-based anode catalyst at 353–373 K can only tolerate traces of CO (<10 ppm) [6]. 10 ppm is the upper limit but it is recommended to reduce the concentration as much as possible to increase the lifetime of the cell anode.

Generally, after the reforming processes, two stages of WGS are necessary for removing most of the CO and producing additional H_2. Consecutive high temperature (573–723 K) and low-temperature (473–573 K) WGS converters are therefore used to reduce the CO content first to 3–5% and then around 0.3–1%, respectively [7]. In order to achieve a hydrogen purity suitable for PEM fuel cell applications, a further purification step is needed based on CO preferential oxidation (COPrOx) [8] or pressure swing adsorption (PSA) [9,10].

Recently, membrane technologies have become increasingly attractive for separation processes due to their modularity and energy efficiency. In particular, membrane reactors are devices combining a chemical reactor and a permselective membrane. In this way, it is possible to reduce sizes and costs (only one device instead of a reactor and a purification train) and increase the reliability of the whole process.

Furthermore, the use of a membrane selective to one of the reaction products (i.e. hydrogen) allows its continue removal, thus promoting the reaction conversion even beyond equilibrium values. Therefore, an interesting alternative is to conduct the WGSR in a membrane reactor (MR) using a membrane selective to hydrogen by operating at high temperature (673–723 K), which allows both high reaction and permeation kinetics to be achieved. In this way, the size of the equipment needed for purification is reduced and the CO conversion increased above equilibrium producing two valuable streams: one of them consists of 100% pure hydrogen (permeate) and the other is rich in CO_2 suitable for sequestration (retentate).

A durable membrane with high selectivity and permeability and a compatible catalyst are two key elements for the efficient operation of the reactor. This concept has been emphasized in a recent review [11]. In this case, besides the assumed attributes of not promoting methanation, high activity and stability, the catalyst should not form carbonaceous residues. These features are

* Corresponding author. Tel.: +54 3424536861; fax: +54 3424536861.
E-mail address: nfisico@fiq.unl.edu.ar (E.A. Lombardo).

0926-860X/$ – see front matter © 2013 Elsevier B.V. All rights reserved.
http://dx.doi.org/10.1016/j.apcata.2013.04.019

particularly critical in the case of a fuel processor used to produce pure H_2 in situ to feed a PEM fuel cell [12]. Several studies of the WGS reaction in Pd membrane reactors have been reported in the literature [13–20]. They were conducted using the commercial Fe-Cr catalyst and noble metal formulations while other publications showed modeling procedures and calculated data without confronting them with experimental results.

Conventional high-temperature WGS catalysts based on Fe-Cr oxides are widely used in industrial processes owing to their low cost, long life, and acceptable sulfur tolerance. Cr_2O_3 is widely used as a stabilizer in industrial WGS catalysts. Iron oxide phases, FeO, Fe_2O_3, and Fe_3O_4, constitute the active system which operates via an oxidation–reduction regenerative mechanism. Hence, the process requires careful control of temperature, H_2O/H_2 and CO_2/CO ratios for (a) securing the equilibrated presence of iron oxides, (b) impairing the reduction of Fe oxides to Fe, which leads to methanation, and (c) avoiding water condensation, which damages chromium oxides [21,22]. Due to the low activity of Fe-Cr oxide catalysts, high reaction temperatures and large reactor volumes are needed. Therefore, noble-metal supported formulations have been investigated as promising next-generation WGS catalysts because they exhibit much faster kinetics compared to conventional ones [7,23]. In addition, these catalysts offer other significant advantages such as no need of activation prior to use, probable no degradation on exposure to air or temperature cycles which could result in the reduction of reactor size and other costs. In this way, options for increasing the activity of Fe-Cr oxides were explored using base metal and noble metal promoters, among which Rh was found to be the most active promoter for Fe-Cr oxides and for Cr_2O_3 [24,25]. However, the substitution of Cr with less harmful components (free chromium catalysts) is desirable due to the environmental concerns related to Cr. Consistent with this analysis, a very active $Rh/La_2O_3.SiO_2$ catalyst was recently reported [26]. Nevertheless, this catalyst promotes the production of methane even when it is used in a membrane reactor.

Trimm and co-workers [25] showed that Rh and Pt have a very similar WGS activity when supported on Cr_2O_3. However, they did not provide information about the methanation activity of these formulations. Obviously, the production of methane is undesirable but even more so when environmental problems arise, e.g. for applications in the fusion fuel cycle where Pd-membrane reactors are studied for the treatment of tritiated water [27]. In such applications, tritium-containing water and CO are converted into hydrogen isotopes and CO_2. The presence of side reactions such as the formation of methane produces a contaminated waste (tritiated methane), thus spoiling the detritiation efficiency of the membrane device. On the other hand, certain platinum formulations do not catalyze methanation, however, a key unsolved problem is its rapid deactivation [7].

The goal of this work was to develop a WGS catalyst with minimal methanation activity, very stable with no carbon formation, suitable for use in a membrane reactor operating at lower hydrogen partial pressure (H_2 permeation) than conventional reactors under similar conditions.

2. Experimental

2.1. Catalyst preparation

The $La_2O_3(27)\cdot SiO_2$ support was prepared by incipient wetness impregnation of SiO_2 (Aerosil 300) with lanthanum nitrate (Sigma–Aldrich, 99.9%). The SiO_2 employed in the support preparation was previously calcined at 1173 K. The La loading was 27.0 wt% of La_2O_3. The $Pt(0.6)/La_2O_3(27)\cdot SiO_2$ catalyst was prepared by incipient wetness impregnation of the support using $Pt(NH_3)_4\cdot Cl_2\cdot H_2O$ as precursor compound. The sample was kept at room temperature for 4 h and then dried at 343 K overnight. The metal load was 0.6 wt%.

2.2. Catalyst characterization

2.2.1. H_2 chemisorption

The metal dispersion of the fresh catalyst, following the in situ hydrogen reduction at 673 K for 1 h, was determined by adsorption of H_2 at 298 K in a conventional vacuum system.

2.2.2. X-ray diffraction (XRD)

The fresh and used solids were analyzed by X-ray diffraction using an XD-D1 Shimadzu instrument and Cu Kα radiation at 30 kV and 40 mA. The scanning rate was 1.0°/min for values between $2\theta = 10°$ and 60°.

2.2.3. Laser Raman spectroscopy (LRS)

The Raman spectra of fresh and used solids were recorded using a LabRam spectrometer (Horiba-Jobin-Yvon) coupled to an Olympus confocal microscope (a 100× objective lens was used for simultaneous illumination and collection), equipped with a CCD detector cooled to about 200 K using the Peltier effect. The excitation wavelength was in all cases 532 nm (Spectra Physics diode pump solid state laser). The laser power was set at 30 mW.

2.2.4. X-ray photoelectron spectroscopy (XPS)

The XPS measurements were carried out using a multitechnique system (SPECS) equipped with a dual Mg/Al X-ray source and a hemispherical PHOIBOS 150 analyzer operating in the fixed analyzer transmission (FAT) mode. The spectra were obtained with pass energy of 30 eV; the Mg Ka X-ray source was operated at 200 W and 12 kV. The working pressure in the analyzing chamber was less than 5.9×10^{-7} Pa. The XPS analyses were performed on the solids after treatment with hydrogen at 673 K carried out in the reaction chamber of the spectrometer.

2.3. Catalytic measurements

The Pt catalyst was first tested in a conventional fixed-bed reactor with the purpose of evaluating its catalytic activity, selectivity and carbon formation. Subsequent tests were carried out in a membrane reactor.

2.3.1. Conventional fixed-bed reactor

For the stability and activity tests, kinetic measurements were conducted in a conventional catalytic fixed-bed reactor isothermally operated at atmospheric pressure. The feed stream gas mixture was made up of 9% CO, 9–27% H_2O and Ar (balance). The catalysts (8 mg) were diluted with inert powder quartz (32 mg) to avoid channeling effects. The reaction was carried out at 673 K and 100 kPa. The reactor was operated at both differential and integral modes.

Prior to use, the Pt catalyst was heated in Ar (1.5 K min^{-1}) at 673 K and then reduced in situ in flowing H_2 at the same temperature for 2 h. On the other hand, the commercial Fe-Cr catalyst was heated in Ar (0.83 K min^{-1}) at 573 K. Then, it was reduced at the same temperature for 2 h under flowing gas made up of 10% CO, 1% H_2O and Ar (balance). CO and Ar were fed through MKS mass flow controllers; steam was generated in a preheater fed with water from a syringe pump (Apema S.R.L.) at the desired flow rate. The gases leaving the reactor flowed through an ice-cooled trap and a tube packed with silica gel to remove water before the gas chromatographic analysis. The feed and product streams were analyzed with a Shimadzu 9A thermal conductivity detector (TCD) gas

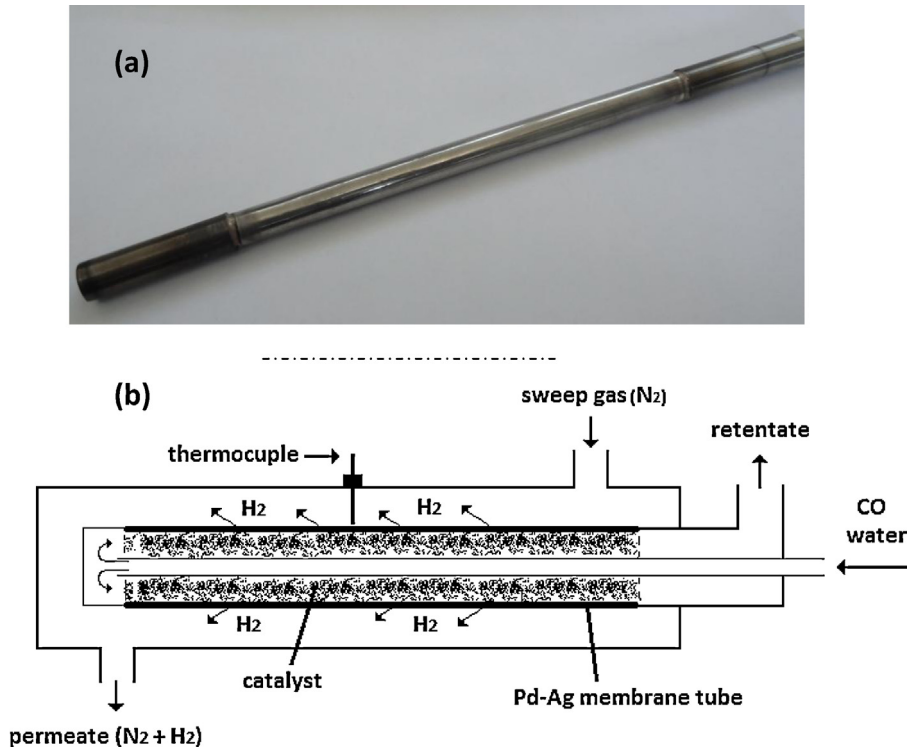

Fig. 1. (a) Pd-Ag membrane tube. (b) Scheme of the Pd-membrane reactor.

chromatograph equipped with a Hayezep D column for the complete separation of the gaseous components.

2.3.2. Membrane reactor

To test the catalyst in a membrane reactor (MR), it was decided to use a self-supporting Pd-Ag membrane with infinite selectivity to H_2, which should be stable for a long time on stream (>1000 h) to avoid the generation of misleading results due to membrane deterioration that would impair the correct evaluation of the catalyst performance in the MR. Besides, as it was required to work up to 1000 kPa, the thickness of the membrane was calculated to avoid accidents. Note that temperatures ≥673 K and pressures above 100 kPa strongly affect the selectivity and stability of one of the best Pd-Ag composite membranes [28].

The membrane reactor was built at the ENEA laboratory using a commercial Pd-Ag (77–23%) membrane tube of diameter 10 mm, length 133 mm, and wall thickness 150 μm. This membrane was defect-free and 100% selective, so only hydrogen was detected on the permeate side. The membrane was brazed to two stainless steel tubes (brazing upper temperature limit 723 K) (Fig. 1a). The Pt(0.6)/La_2O_3(27).SiO_2 catalyst (1.5 g), diluted with quartz wool (2 g), to achieve a height of 133 mm was packed inside the membrane lumen between two quartz wool stoppers.

The membrane was assembled in a finger-like configuration into a Pyrex module (shell side) according to a well-proven membrane reactor design [29]. A thermocouple to measure the temperature was placed in the middle of the permeator tube on its external surface (Fig. 1b).

The membrane device was characterized in permeation mode. During the permeation tests, hydrogen was fed into the membrane lumen: the hydrogen permeability was assessed by measuring the permeation flux under controlled temperature and pressure conditions. In the reaction tests, the feed stream gas mixture consisted of H_2O and CO. CO was fed through a MKS mass flow controller; the steam was generated by vaporizing a water stream fed via a Brooks liquid mass flow controller. The catalyst was heated in N_2 at 673 K and then reduced in situ by flowing H_2 at the same temperature for 2 h. The reaction was carried out at 673–723 K in the pressure range 100–800 kPa.

In both permeation and reaction experiments, the hydrogen permeated through the membrane was collected by a sweep stream of nitrogen fed in counter-current at varying flow rates from 0 to 700 N mL min^{-1}. In actual practice, overheated steam is used to facilitate H_2 separation from the sweep gas.

The gases leaving the membrane lumen (retentate) flowed through a condenser which removed its liquid fraction before going to the gas chromatographic analysis. The feed and retentate streams were analyzed with an Agilent 7820 A gas chromatograph using a thermal conductivity detector (TCD) and a flame ionization detector (FID). The instrument was equipped with two columns HP-MOLESIEVE (serial number USB676327H) and GS-CARBONPLOT (USB577416H) for the complete separation of the gaseous components. From time to time, the permeate stream (without sweep gas) was analyzed using a quadrupole mass spectrometer. The detection limit of H_2 impurities was ca. 10 ppm.

3. Results and discussion

3.1. Catalyst characterization

The X-ray diffraction patterns of the support indicated that the solid was made up of a low crystallinity disilicate ($La_2Si_2O_7$) and SiO_2. The reflection angles (2θ) observed and their corresponding phases are shown in Table 1. The $La_2Si_2O_7 \cdot SiO_2$ formulation was reported elsewhere [30–32].

Not even a trace of La_2O_3 was detected by either XRD or Raman spectroscopy in fresh and used catalysts (Table 1). Furthermore, if the oxide were present it would react with CO_2 while on stream, forming carbonates easily detectable through Raman Spectroscopy [31]. In fact, the Raman spectra of the used Pt(0.6)/La_2O_3(27)·SiO_2 catalysts do not show bands corresponding to the presence of either

Table 1
Phases observed in both catalysts, fresh and used, through XRD and LRS.

Catalyst	Phases	Reflections (2θ)	Raman 200–1600 cm^{-1} region
Pt/La_2O_3·SiO_2 fresh and used[a]	$La_2Si_2O_7$ SiO_2 graphite	28, 45 (b.p.)[b] 23 (b.p.)[b] undetected	no signals no signals Undetected

[a] After WGS reaction, feeding 9% CO, 27% H_2O and Ar (balance) at 673 K for 50 h.
[b] b.p.: broad peaks.

carbonates or graphitic residues. Note that this spectroscopic tool is very sensitive to the presence of graphitic residues.

A BET surface area of 180 m^2 g^{-1} was measured for the catalyst. The metal dispersion of the fresh reduced solid calculated from H_2 chemisorption was 16% and the bulk density was 0.5 g mL^{-1}.

3.1.1. XPS data

The binding energies of fresh reduced and used Pt(0.6) samples are reported in Table 2. The Pt 4f $_{7/2}$ binding energies for both samples at 71.0 ± 0.2 eV indicate that Pt is present as Pt°. Besides, a second Pt component is observed at higher binding energies (73.9 ± 0.3 eV) corresponding to an oxidized species. This signal could be assigned to a Pt^{4+} species [33] which could arise from an incomplete decomposition and oxidation of the Pt precursor.

Note that, on the reduced catalyst, not all the Pt exposed was present as Pt° (86.9%) and this value decreased to 76.1% after its exposure to WGS atmosphere. Pt species could be oxidized under the WGS conditions (H_2O/CO = 3).

For the reduced and used catalysts, the XPS intensity ratios of La 3d$_{5/2}$/Si 2s, Pt 4f $_{7/2}$/Si 2s and O 1s/Si 2s remained unchanged (Table 2). As the surface Pt 4f $_{7/2}$/Si 2s ratio was practically the same before and after the WGS reaction, this could indicate that the Pt dispersion did not change. This is consistent with the constant activity of the catalyst recorded during the 155 h stability test (vide infra).

3.2. Catalyst activity measurements and comparison with literature data

3.2.1. Stability test

The test was designed to include several start-ups and shut-downs of the reaction system. This is an important feature of the catalyst to be used either in a fuel processor or in a membrane reactor. The test was carried out in a conventional fixed-bed tubular reactor (5 mm i.d). Fig. 2 shows the data obtained for the Pt catalyst under different WGS conditions (H_2O/CO = 1–3, GHSV = 1.2–1.5 × 10^6 h^{-1}) at 673 K, 100 kPa. Note that the catalyst resulted stable under the different WGS feed compositions (H_2O/CO = 1–3). Between shut-down and start-up cycles, the catalyst was exposed to flowing Ar at either 673 K or 298 K. The results show that the stability of the Pt catalyst was not affected by these cycles. No methane was detected during the test.

In order to compare the catalytic activity of the Pt(0.6)/La_2O_3.SiO_2 catalyst with a commercial one, the reaction

Table 2
Binding energies (eV) and surface atomic ratios of fresh (reduced) and used (after WGSR) Pt(0.6)/La_2O_3.SiO_2 catalysts.

Catalyst	Treatment	Binding energies (eV)[a]				Surface atomic ratios		
		La 3d$_{5/2}$	O 1s	Si 2s	Pt 4f$_{7/2}$	La 3d$_{5/2}$/Si 2s	Pt 4f $_{7/2}$/Si 2s	O 1s/Si 2s
Pt(0.6)/La_2O_3·SiO_2	Reduced	835.1	532.3	154.1	70.9 (86.9)[b] 73.6 (13.1)[b]	0.15	0.0022	2.4
	Used in WGSR	835.2	532.0	154.0	71.2 (76.1)[b] 74.0 (23.9)[b]	0.13	0.0023	2.7

[a] Contamination carbon was taken as reference at 284.6 eV.
[b] The relative percent of platinum species is given in parentheses.

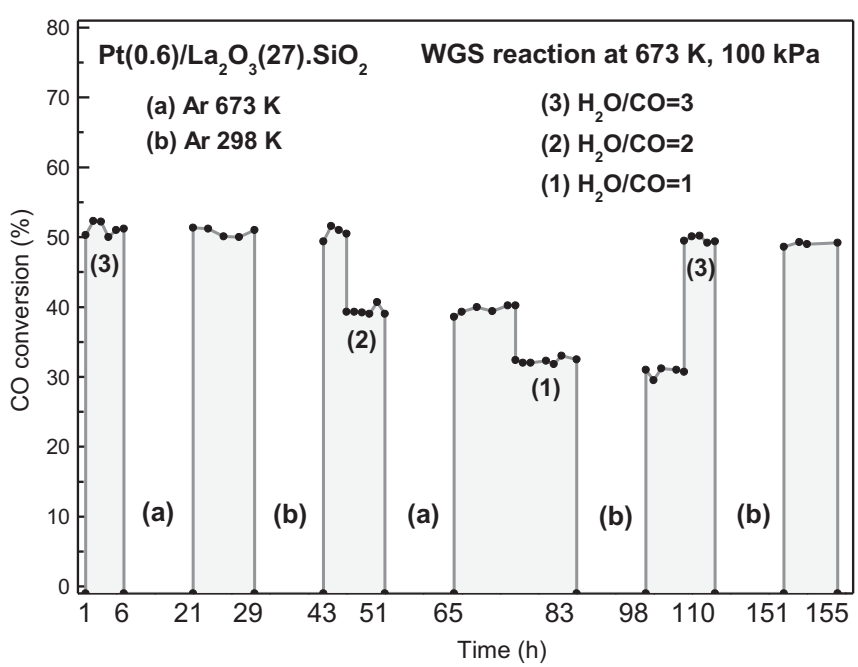

Fig. 2. Stability test. CO conversion vs time including start-up and shut-down cycles of WGS reaction over Pt(0.6)/La_2O_3(27)·SiO_2 catalyst at 673 K, 100 kPa, H_2O/CO = 1–3, GHSV = 1.2–1.5 × 10^6 h^{-1}.

Table 3
Comparison of catalytic behavior: High temperature WGS catalysts.

Catalysts[a]	D[b] (%)	Stability (673 K)		Rate[c] 673 K	Rate[d] 673 K	H_2O/CO	Reference
		TOS (h)	Decay (%)				
$Pt(0.6)/La_2O_3(27)\cdot SiO_2$	16	155[e]	0	170	28.3	1	This work
	16	155[e]	0	482	80.6	3	This work
Commercial Fe-Cr		[f]	–	40	–	1	This work
		[f]	–	51.7	–	3	This work
		–	–	42	–	1	[23]
$Pt(0.5)/TiO_2$	67	60	0	290	58.0	3.33	[34]
$Pt(0.92)Re(1.79)/Ce_{0.6}Zr_{0.4}O_2$	69	60	20[g]	310	33.5	4.5	[35]
$Pt(1.05)/Ce_{0.46}Zr_{0.54}O_2$	60	60	50[g]	150	14.3	4.5	[35]
$Ce_{0.78}Sn_{0.2}Pt_{0.02}O_{2.5}$ (2.3 wt% Pt)		90[h]	0	149[i]	6.48	6.6	[36]
$Pt(0.5)/Yb\text{-}CeO_2$	40	–	–	738[j]	147[j]	3.3	[37]
$Pt(0.5)/CeO_2$	46	–	–	323[j]	64.6[j]	3.3	[37]
$Pt(1.0)/Cr_2O_3$[k]	–	–	–	105[l]	10.5[l]	1	[25]
$Rh(0.6)/La_2O_3(27)\cdot SiO_2$	79	50	0	270	45.0	3	[26]
$Rh(1.0)/Fe_2O_3\text{-}Cr_2O_3$	–	–	–	165	16.5	1	[23]

[a] The weight percent of the noble metals and La_2O_3 are indicated between parentheses.
[b] Dispersion.
[c] μmol CO converted. $g_{cat}^{-1}\ s^{-1}$.
[d] mmol CO converted. $g_{NM}^{-1}\ s^{-1}$ (NM = Pt or Rh).
[e] Besides, no deactivation was observed during start-up/shut-down cycles for at least 155 h (Fig. 2).
[f] Stability of at least one year reported by industry.
[g] Test conducted at 573 K.
[h] Stability of 90 h reported in Ref [36] reflects behavior at 100% conversion (doubtful).
[i] Extrapolated using E_{act} = 20 kcal mol^{-1} average from [37].
[j] Calculated from rate data at 523 K using the activation energies provided by the authors.
[k] These authors also used as supports: $Cr_2O_3\text{-}Fe_3O_4$, $CeO_2\text{-}ZrO_2$, CeO_2, MgO V_2O_5, ZrO_2, Fe_3O_4, MoO_3, MuO_2, Al_2O_3, Bi_2MoO_6, with 1% Pt. None of these formulations was more active than 1% Pt/Cr_2O_3.
[l] Calculated from rate data at 723 K using the activation energies provided by the authors.

was carried out for both solids at 673 K, 100 kPa, H_2O/CO = 1–3, and GHSV = $2.8 \times 10^6\ h^{-1}$ operating in differential mode (X_{CO} < 10%). Table 3 shows that the reaction rates of the Pt catalyst were 9.4 and 4.1 times higher than those of the commercial catalyst with a H_2O/CO ratio of 3 and 1, respectively. This is a valuable result since several authors have reported the necessity of finding a more active, stable, selective and non-carbon forming catalyst to use in membrane reactors [13,14].

After the entries corresponding to this work the next four catalysts listed in Table 3 include some stability data. They are presented in descending activity per gram of Pt. $Pt(0.5)/TiO_2$ seems to be the best one but still less performant than $Pt(0.6)/La_2O_3.SiO_2$. However, the difference between $Pt(0.5)/TiO_2$ and another similar Pt/TiO_2 formulation reported in the literature [38] that rapidly deactivates is not clear. Maybe the different precursors and/or drying-calcination steps are responsible for the different stabilities. Note that the stability test reported by Gupta and Hegde [36] is not convincing because they show results of on-off runs where the conversion is ca. 100% instead of selecting values in the middle third of the conversion scale.

The following three Pt formulations do not provide information about stability. Maybe $Pt(0.5)/Yb\text{-}CeO_2$ could outperform ours if this catalyst could also maintain its activity for more than 150 h under a similar stability test protocol.

The catalytic activities of Rh-containing formulations are also reported in Table 3. The $Rh(1.0)/Fe_2O_3\text{-}Cr_2O_3$ [23] and $Pt(0.6)/La_2O_3(27).SiO_2$ catalysts show similar catalytic activity per gram of catalyst at H_2O/CO = 1. However, the reaction rate of the Pt formulation per gram of noble metal is 4.9 times higher than the $Rh(1.0)/Fe_2O_3\text{-}Cr_2O_3$ catalyst. Furthermore, the Fe-Cr catalysts require a careful control of the operating variables; otherwise, the catalysts could be destabilized with several consequences: changes of the active phase (Fe_3O_4), low reaction rate, methane formation and carbon deposition. Although the Rh(0.6 wt%)/La_2O_3(27 wt%).SiO_2 formulation is stable for at least 50 h on stream it produces more than 15% CH_4 at CO conversions above 90%.

In brief, at H_2O/CO = 3, the $Pt(0.6)/La_2O_3\cdot SiO_2$ is more active than all but one of the catalysts reported in Table 3 and it is the most stable one of the Pt series. Of course, months-long runs of the Pt catalyst are needed to check its stability against the commercial $Cr_2O_3\cdot Fe_3O_4$ formulation.

3.3. Thermodynamic analysis

Although the WGS reaction carried out by a membrane reactor in a dynamic mode can reach conversion values beyond equilibrium, the thermodynamic analysis can provide some guidance concerning the feasibility of secondary, undesirable reactions. Fig. 3 shows the calculated equilibrium values of CO conversion and CH_4

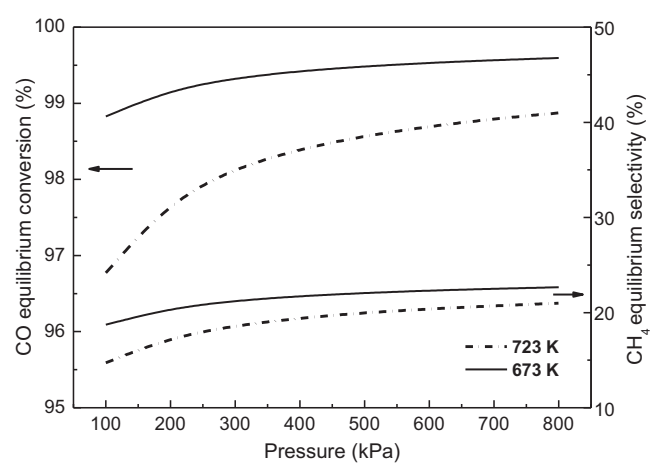

Fig. 3. Equilibrium values of the CO conversion and CH_4 selectivity at different pressures and temperatures, and H_2O/CO = 2.

selectivity at different pressures, when the reaction is carried out at 623 and 673 K and with a $H_2O/CO = 2$ ratio. As the tests described in the previous sections demonstrated that this catalyst does not produce carbon containing residues, the thermodynamic analysis was performed leaving out its formation.

The reactions considered for these calculations are:

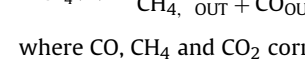

$$CO + H_2O \leftrightarrow CO_2 + H_2$$

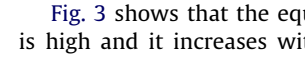

$$CO_x + (2+x)H_2 \leftrightarrow CH_4 + xH_2O$$

The CH_4 selectivity (Se_{CH_4}) was calculated as:

$$Se_{CH_4}(\%) = \frac{CH_{4,\ OUT}}{CH_{4,\ OUT} + CO_{OUT} + CO_{2,\ OUT}} \times 100 \quad (1)$$

where CO, CH_4 and CO_2 correspond to the molar concentration of these compounds.

Fig. 3 shows that the equilibrium value of the CH_4 selectivity is high and it increases with pressure. Such a driving force for methanation should be neutralized using an appropriate catalyst to prevent this reaction under the operation conditions that favor the WGS reaction.

In a membrane reactor, the CH_4 selectivity values obtained should be lower than the thermodynamic ones due to the catalyst used and the H_2 permeation through the membrane.

3.4. Membrane reactor

The Pd-Ag membrane was first characterized and then, the WGS catalytic tests were carried out under different reaction conditions.

3.4.1. Permeation tests

The Pd membrane was characterized in terms of hydrogen permeability and selectivity. The hydrogen permeation flux through a dense palladium membrane can be expressed as follows [39]:

$$J_{H_2} = \frac{P_E}{d}(P^n_{H_2,R} - P^n_{H_2,P}) \quad (2)$$

where J_{H_2} is the gas flux (mol m^{-2} s^{-1}), P_E is the permeability of the membrane (mol m^{-1} s^{-1} Pa^{-n}), d is the membrane thickness (m), n is the pressure exponent, $P_{H_2,R}$ and $P_{H_2,P}$ are the H_2 partial pressure in the retentate and in the permeated side of the membrane, respectively. The value of n is often used as an indicator for the rate-controlling step. Under the operating conditions of this work the value of n is 0.5 (Sieverts' law) [40] hinting that the diffusion of atomic hydrogen through the membrane is rate-controlling.

In order to calculate the permeability, pure hydrogen was fed into the membrane module and a constant sweep gas flow rate (500 N mL min^{-1}) of N_2 was used in the permeate side for collecting the hydrogen permeated through the membrane. The reactor was operated in counter-current mode to maximize the permeation driving force profile.

Since pure hydrogen is fed into the membrane lumen and the pressure drop can be neglected, the H_2 partial pressure in the retentate (lumen) side is constant and equal to the feed pressure. Conversely, in the shell side the H_2 partial pressure increases along the reactor axis as a consequence of the hydrogen permeated. By considering the analogy between mass and heat transfer, the driving force of the hydrogen permeation can be expressed similarly to the temperature driving force (log mean temperature difference) of a heat exchanger. In this way, the hydrogen permeation flux J_{H_2} is given by Eq. (2):

$$J_{H_2} = \frac{P_E}{d}.\Delta P^{0.5}_{HL} = \frac{P_E}{d}.\frac{P^{0.5}_{H_2,P}}{\ln[P^{0.5}_{H_2,R}/(P^{0.5}_{H_2,R} - P^{0.5}_{H_2,P})]} \quad (3)$$

where $\Delta P_{HL}{}^{0.5}$ (Pa$^{0.5}$) means the half logarithmic pressure drop. Note that the $P_{H_2,P}$ values were calculated by considering the H_2 flow permeated and the sweep gas used.

The experimental data of the H_2 permeation flux were successfully fitted ($R^2 = 0.999$) using Eq. (2): a P_E value of 1.38×10^{-8} mol s^{-1} m^{-1} Pa$^{-0.5}$ was obtained at 673 K.

To calculate the temperature dependence of the permeability, experimental data were obtained between 623 and 723 K and at 100 kPa (using the Eq. (2)). These values were then fitted using an Arrhenius-type equation:

$$P_E = P^\circ{}_E.e^{[-E_A/RT]} \quad (4)$$

where $P^\circ{}_E$ is the permeability pre-exponential coefficient (mol m^{-1} s^{-1} Pa$^{-0.5}$) and E_A the activation energy (J mol^{-1}).

The Arrhenius equation exhibited a correlation factor $R^2 = 0.974$, $P^\circ{}_E$ of 3.46×10^{-8} mol m^{-1} s^{-1} Pa$^{-0.5}$ and E_A of 5100 ± 130 J mol^{-1}. These permeability E_A values are in agreement with those reported in the literature for similar Pd-Ag membranes [41].

3.4.2. Pd-membrane reactor tests

In order to assess the performance of the Pt(0.6)/La_2O_3(27)·SiO_2 catalyst in the membrane reactor, different runs were performed between 673 and 723 K, with the pressure ranging from 100 kPa to 800 kPa, feed molar ratio $H_2O/CO = 2$ and space velocities of GHSV = 3120, 6240 and 9360 h^{-1} in the retentate side.

The temperature limits were imposed by two factors: (i) $T < 673$ K increases the CO poisoning of the membrane that reduces the hydrogen permeability, (ii) $T > 723$ K shortens the membrane durability because it overtakes the upper operating temperature of the membrane tube brazing.

The performance of the membrane reactor was evaluated in terms of the CO conversion, CH_4 selectivity and hydrogen recovery (R_{H2}). The latter parameter indicating the fraction of H_2 recovered in the permeate side of the membrane reactor was defined as follows:

$$\mathbf{R}_{H_2}(\%) = \frac{H_{2,P}}{H_{2,P} + H_{2,R}} \times 100 \quad (5)$$

where $H_{2,P}$ and $H_{2,R}$ correspond to the hydrogen flow rate (N mL min^{-1}) in the permeate and the retentate side, respectively.

3.4.2.1. Effect of the sweep gas flow rate. In order to find out the sweep gas flow rate required to maximize both the CO conversion and H_2 recovery, the space velocity was fixed at 6240 h^{-1}. The evolution of the CO conversion and H_2 recovery with the sweep gas flow rate is shown in Fig. 4 at GHSV = 6240 h^{-1}, 100–400 kPa and 673–723 K. The CO conversion and H_2 recovery increase with the sweep gas flow rate. In fact, the increase of the sweep gas flow rate reduces the hydrogen partial pressure on the permeate side leading to higher H_2 permeation fluxes through the membrane. However, when the sweep gas flow rate was higher than 500 N mL min^{-1} both the CO conversion and the hydrogen recovery remained practically constant.

In Fig. 4a, without sweep gas at 100 kPa, CO conversion values of 49.7 and 59% are observed at 673 and 723 K, respectively. In these conditions, the membrane reactor approaches the behavior of a conventional fixed-bed reactor. Instead, when the reaction was carried out at 100 kPa with a sweep gas flow rate of 500 N mL min^{-1} which approached plateau conditions, the CO conversion values were about 36 and 26% higher than when the system was operated without sweep gas, at 673 and 723 K, respectively. Without sweep gas and at 400 kPa, the CO conversion values obtained at 673 and 723 K were similar to the values at 100 kPa (Fig. 4a).

Fig. 4b shows the H_2 recovery as a function of the sweep gas flow rate. Note that the effect of pressure is more important than temperature because the H_2 flux through the membrane

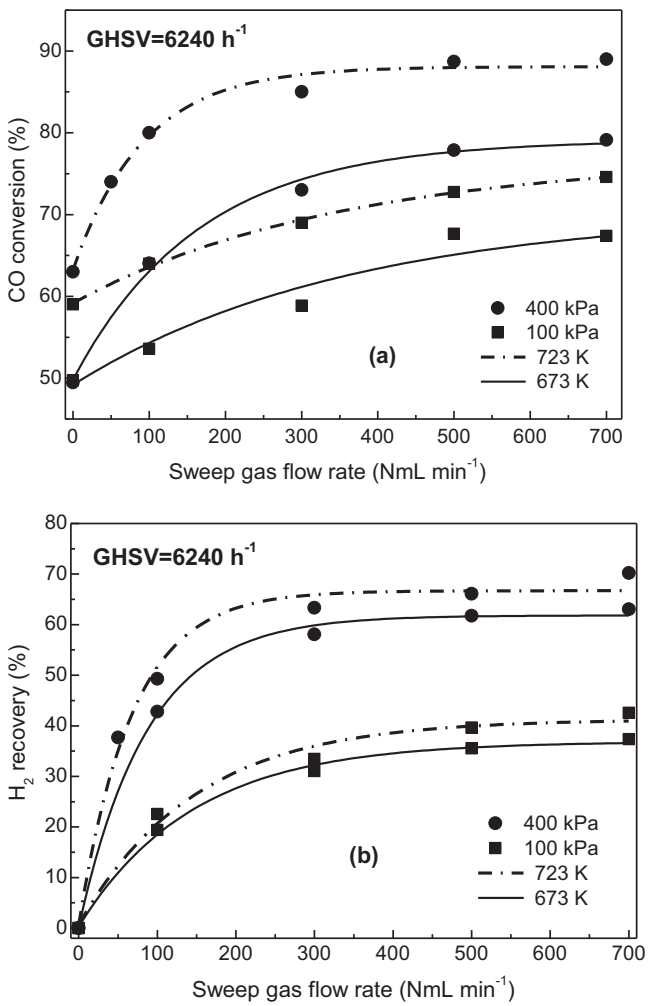

Fig. 4. Effect of the sweep gas flow rate over (a) CO conversion and (b) H_2 recovery, at $H_2O/CO = 2$ ($W_{catalyst} = 1.5$ g).

has low activation energy (5100 J mol^{-1}). The H_2 recovery values at 673 and 723 K remain practically constant when the sweep gas flow rate is higher than 500 N mL min^{-1}. The same conclusion was reached when analyzing the CO conversion behavior (Fig. 4a). Consequently, in subsequent tests, the sweep gas flow rate was fixed at 500 N mL min^{-1} that allowed CO conversion and the hydrogen recovery to reach plateau values at the different GHSVs explored.

3.4.2.2. Effect of the space velocity (GHSV). Fig. 5 compares CO conversion and H_2 recovery as a function of the feed (retentate) pressure for three different space velocities (3120, 6240 and 9360 h^{-1}). The pressure increases the hydrogen permeation through the membrane according to Eq. (2). Therefore, the hydrogen removal through the membrane promotes the CO conversion through the well-known "shift effect".

The significant drop in H_2 recovery is due to the decrease of the reactants residence time. Note that increasing retentate pressure beyond 800 kPa will produce only a small increment in H_2 recovery and almost no effect in CO conversion. Therefore it is concluded that it is not effective to increase the pressure beyond 800 kPa.

Figs. 4 and 5 show a positive temperature effect. This is mainly due to the fact that a higher temperature increases the WGS reaction rate and to a smaller extent the H_2 permeation through the membrane.

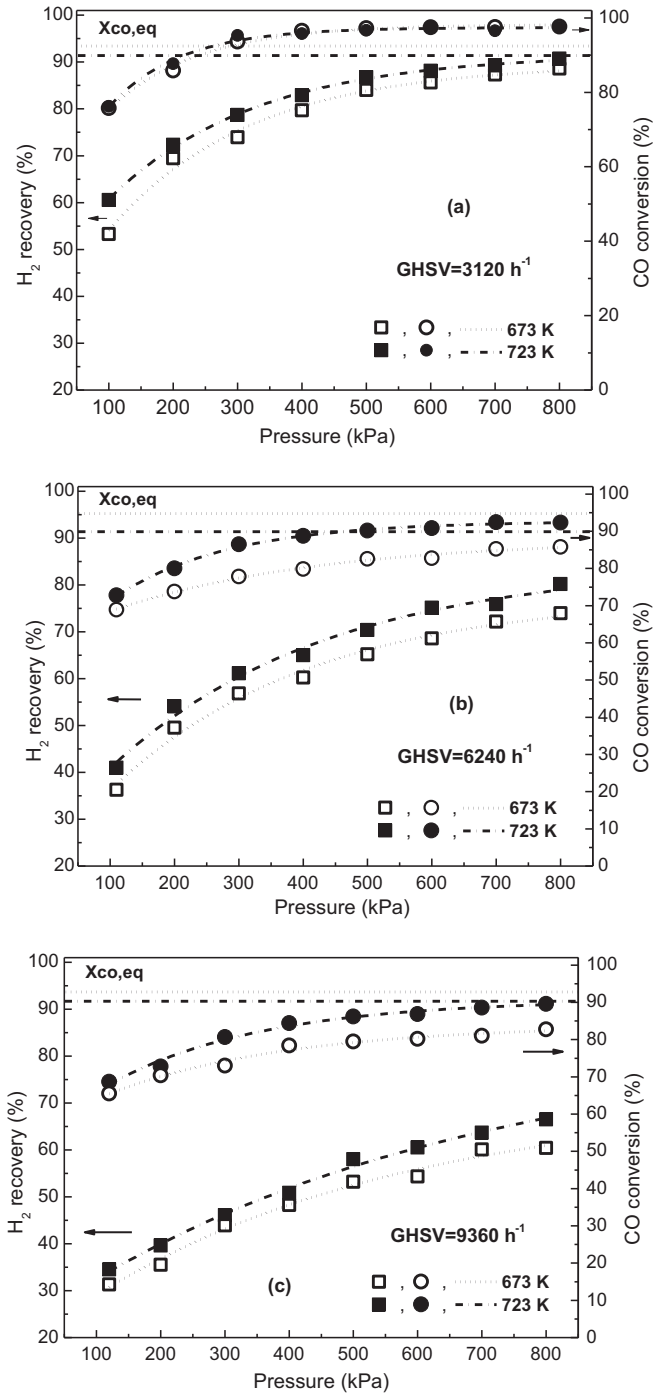

Fig. 5. Effect of pressure and temperature upon the CO conversion and H_2 recovery ($H_2O/CO = 2$), at different space velocities, $F_{SG} = 500$ N mL min^{-1} ($W_{catalyst} = 1.5$ g).

3.4.3. CH_4 selectivity

The CH_4 selectivity values obtained in the membrane reactor at 6240 h^{-1} with a sweep gas flow rate of 500 N mL min^{-1} are shown in Fig. 6. Note that these values are 100 times smaller than the theoretical values calculated under thermodynamic equilibrium conditions. Accordingly, these membrane reactor tests further verified that the Pt(0.6)/La_2O_3(27)·SiO_2 catalyst does not promote methane formation. The maximum CH_4 selectivity value (0.22%) was obtained without sweep gas at 723 K, 400 kPa and operating with a space velocity of 6240 h^{-1}.

The slight maximum at 400–500 kPa of the experimental curves of Fig. 6 could be interpreted as follows: moving from low

Table 4
Comparison of WGS membrane reactors performance.

Membrane	δ[a] (μm)	Catalyst	$T_{reaction}$ (K)	$P_{reaction}$ (kPa)	H_2O/CO (molar)	GHSV (h^{-1})	H_2 prod. flux ($Nm^3\,m^{-2}\,h^{-1}$)	X_{CO}[b] (%)	H_2 Rec[c] (%)	H_2 purity (%)	Ref. #
Pd-Ag[d]	150	$Pt/La_2O_3.SiO_2$	673	800	2	3120	0.55	97.5	88	99.999	This work
			723	800	2	3120	0.62	97.7	90	99.999	This work
			673	800	2	6240	0.96	85.8	75.1	99.999	This work
			723	800	2	6240	1.2	92.3	85.4	99.999	This work
Pd-Ag[d]	60	CuO/CeO_2	573	600	1	3180	–	90	75	99.999	[17]
Pd-Ag[d]	50	Fe_3O_4/Cr_2O_3[e]	598	100	1.5	1307[f]	0.25	98.9	71	99.999	[15]
Pd/PSS	29	Fe_3O_4/Cr_2O_3[e]	683	600	3.6	1003	2.97	85.0	82.0	97.0	[42]
Pd/PSS	20	Fe_3O_4/Cr_2O_3[e]	663	1100	3	3450	–	85	66	95	[16]
Pd-Ag/PInconel	8.8	Fe_3O_4/Cr_2O_3[e]	723	1440	1.6	5502	9.74	93.6	78.1	99.9[g]	[19]
Pd/PSS	8.3	Fe_3O_4/Cr_2O_3[e]	713	2000	2.5	5650	11.67	84.9	42.8	99.5	[20]
Pd/CS[h]	1.4	$Pt/Ce_{0.6}Zr_{0.4}O_2$	623	1200	2.9	14,100	27.95	94.9	48.7	99.7	[14]

[a] Pd or Pd-Ag thickness.
[b] CO conversion.
[c] H_2 recovery.
[d] Self standing.
[e] Commercial formulations.
[f] Value estimated from data provided by one of the authors.
[g] Estimated from ideal selectivity data provided in reference [19].
[h] Ceramic support (CS).

pressures, an increase of P_{H_2} enhances the methanation while at higher pressure, by increasing the reaction pressure, the hydrogen partial pressure decreases due to higher hydrogen permeation flow rate, in this way decreasing the methanation activity.

The explanation of the opposing temperature effect upon the equilibrium and kinetic methane selectivity can be found in the difference between the activation energy of the methanation reaction and that of the hydrogen transport through the membrane, the former being obviously higher than the latter.

3.4.4. Comparison with published data

Several factors should be considered when comparing the performances of WGS membrane reactors. The most important ones are CO conversion, H_2 recovery, H_2 purity, H_2 production ($kg\,h^{-1}\,m^{-2}$) and stability. Our membrane is by far more stable than composite membranes but the permeability ratio is inverted. Another key factor is the extent of the unwanted methanation reaction often ignored in most publications.

Caution should be exercised when analyzing literature data because those experiments run at $T < 673$ K could include the negative effect of CO adsorption on the membrane upon the H_2 permeance.

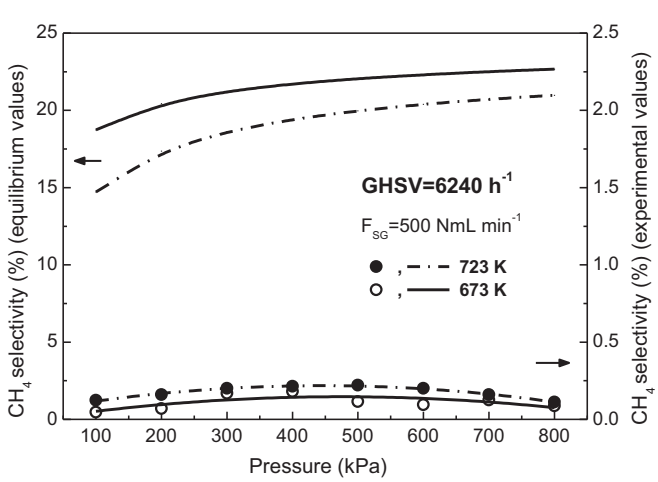

Fig. 6. CH_4 selectivity for the $Pt(0.6)/La_2O_3(27)\cdot SiO_2$ catalyst in the membrane reactor ($W_{catalyst}$ = 1.5 g). Comparison with equilibrium values.

Table 4 includes a selection of articles published between 2003 and 2013 showing the best performance of membrane reactors available. The reaction temperature varies between 573 K and 723 K while the retentate pressures goes from 100 kPa to 1440 kPa. The reactors were built with either self-standing supported or composite Pd or Pd-Ag membranes. Mainly commercial Cr-Fe catalysts were used.

As expected, the highest H_2 purity was obtained with self-standing Pd-Ag membranes. Not shown in Table 4 is the selectivity decay with TOS often observed with composite membranes and not with self-standing films. High CO conversions can be achieved with both types of membranes. Concerning H_2 recoveries, note that the values are generally lower with composites with the aggravating factor that in the latter case the H_2 permeated does not reach the purity required to feed PEM fuel cells.

The H_2 production flux is another key parameter and, as expected, it increases sharply for composites due not only to the thinner metal layers but also to the existence or development during use of pinholes and/or cracks in the alloy film. This, in turn, negatively affects the H_2 purity.

4. Conclusions

The $Pt(0.6)/La_2O_3(27)\cdot SiO_2$ formulation is probably the most active and stable high temperature WGS catalyst reported in the literature so far. Furthermore, this catalyst exhibits very low methanation selectivity. Kinetic measurements carried out in a conventional reactor indicate that the methanation activity is still very low when the hydrogen concentration in the reacting stream goes up to 60%. Rh or $Ru/La_2O_3\cdot SiO_2$ formulations are also very stable under the more severe dry reforming conditions (823 K, 100 kPa) [31,43]. In view of the dispersion constancy before and after use it is concluded that an optimized metal support interaction is at least partially responsible for the high activity and stability of noble metal formulations supported on $La_2O_3\cdot SiO_2$ calcined at 873 K. Note that after calcination at 873 K, the support is made up of $La_2Si_2O_7$ and SiO_2 with no free La_2O_3.

The catalyst was tested in a membrane reactor using a dense, defect-free Pd-Ag tube which allowed 99.999% pure hydrogen to be produced at high CO conversion (up to 98%) consistent with the "shift effect" allowed by the membrane. At 723 K and GHSV = 6240 h^{-1}, the CO conversions approaching or overcoming the equilibrium ones were achieved by operating the Pd-membrane

reactor at 800 kPa. Under these operating conditions the hydrogen recovery was 80%, the CO conversion was 92% and the H_2 production was 1.18 $Nm^3\,h^{-1}\,m^{-2}$, a value in line with similar systems reported in the literature.

Acknowledgments

The authors wish to thank Universidad Nacional del Litoral (UNL), Consejo Nacional de Investigaciones Científicas y Tecnológicas (CONICET), Università di Roma "La Sapienza" and the Erasmus program for the financial support. Thanks are also given to Elsa Grimaldi for the English language editing. C.A.C. also thanks the ENEA laboratories for the generous hospitality.

References

[1] V.A. Goltsov, T.N. Veziroglu, Int. J. Hydrogen Energy 26 (2001) 909–915.
[2] J. Barton, R. Gammon, J. Power Sources 195 (2010) 8222–8235.
[3] P. Moriarty, D. Honnery, Int. J. Hydrogen Energy 35 (2010) 12374–12380.
[4] J.D. Holladay, J. Hu, D.L. King, Y. Wang, Catal. Today 139 (2009) 244–260.
[5] A.L. Dicks, J. Power Sources 61 (1996) 113–124.
[6] R. Buxbaum, H. Lei, J. Power Sources 123 (2003) 43–47.
[7] C. Ratnasamy, J.P. Wagner, Catal. Rev. 51 (2009) 325–440.
[8] N. Bion, F. Epron, M. Moreno, F. Mariño, D. Duprez, Top. Catal. 51 (2008) 76–88.
[9] F.V.S. Lopes, C.A. Grande, A.E. Rodrigues, Chem. Eng. Sci. 66 (2011) 303–317.
[10] Q. Huang, A. Malekian, M. Eić, Sep. Purif. Technol. 62 (2008) 22–31.
[11] K. Babita, S. Sridhar, K.V. Raghavan, Int. J. Hydrogen Energy 36 (2011) 6671–6688.
[12] X. Liu, W. Ruettinger, X. Xu, R. Farrauto, Appl. Catal. B: Environ. 56 (2005) 69–75.
[13] D. Ma, C.R.F. Lund, Ind. Eng. Chem. Res. 42 (2003) 711–717.
[14] Y. Bi, H. Xu, W. Li, A. Goldbach, Int. J. Hydrogen Energy 34 (2009) 2965–2971.
[15] S. Tosti, A. Basile, G. Chiappetta, C. Rizzello, V. Violante, Chem. Eng. J. 93 (2003) 23–30.
[16] S. Liguori, P. Pinacci, P.K. Seelam, R. Keiski, F. Drago, V. Calabrò, A. Basile, A. Iulianelli, Catal. Today 193 (2012) 87–94.
[17] G. Barbieri, A. Brunetti, G. Tricoli, E. Drioli, J. Power Sources 182 (2008) 160–167.
[18] A. Basile, G. Chiappetta, S. Tosti, V. Violante, Sep. Purif. Technol. 25 (2001) 549–571.
[19] A.S. Augustine, Y.H. Ma, N.K. Kazantzis, Int. J. Hydrogen Energy 36 (2011) 5350–5360.
[20] J. Catalano, F. Guazzone, I. Mardilovich, N. Kazantzis, Y.H. Ma, Ind. Eng. Chem. Res. 52 (2013) 1042–1055.
[21] D.L. Trimm, Appl. Catal. A: Gen. 296 (2005) 1–11.
[22] M.V. Twigg (Ed.), Catalyst Handbook, Wolf Scientific Text, London, 1989.
[23] Y. Lei, N.W. Cant, D.L. Trimm, J. Catal. 239 (2006) 227–236.
[24] C. Rhodes, B. Peter Williams, F. King, G.J. Hutchings, Catal. Commun. 3 (2002) 381–384.
[25] Y. Lei, N. Cant, D. Trimm, Catal. Lett. 103 (2005) 133–136.
[26] C.A. Cornaglia, J.F. Múnera, E.A. Lombardo, Ind. Eng. Chem. Res. 50 (2011) 4381–4389.
[27] S. Tosti, C. Rizzello, in: A. Basile, S.P. Nunes (Eds.), Advanced Membrane Science and Technology for Sustainable Energy and Environmental Applications, Woodhead Publishing Series in Energy, Cornwall, UK, 2011, ISBN 978-1-84569-969-7, pp. 769–791, Ch. 24, ISSN: 2044-9364.
[28] T.A. Peters, W.M. Tucho, A. Ramachandran, M. Stange, J.C. Walmsley, R. Holmestad, A. Borg, R. Bredesen, J. Membr. Sci. 326 (2009) 572–581.
[29] S. Tosti, A. Adrover, A. Basile, V. Camilli, G. Chiappetta, V. Violante, Int. J. Hydrogen Energy 28 (2003) 105–112.
[30] C.A. Cornaglia, J.F. Múnera, L.M. Cornaglia, E.A. Lombardo, P. Ruiz, A. Karelovic, Appl. Catal. A: Gen. 435–436 (2012) 99–106.
[31] S. Irusta, J. Múnera, C. Carrara, E.A. Lombardo, L.M. Cornaglia, Appl. Catal. A: Gen. 287 (2005) 147–158.
[32] H. Vidal, S. Bernal, R.T. Baker, D. Finol, J.A. Pérez Omil, J.M. Pintado, J.M. Rodriguez - Izquierdo, J. Catal. 183 (1999) 53–62.
[33] T. Baidya, A. Gayen, M.S. Hedge, N. Ravishankar, L. Dupont, J. Phys. Chem. B 110 (2006) 5262–5272.
[34] P. Panagiotopolou, D.I. Kondarides, Appl. Catal. B: Environ. 101 (2011) 738–746.
[35] S.Y. Choung, M. Ferrandon, T. Krause, Catal. Today 99 (2005) 257–262.
[36] A. Gupta, M.S. Hegde, Appl. Catal. B: Environ. 99 (2010) 279–288.
[37] P. Panagiotopoulou, J. Papavasiliou, G. Avgouropoulos, T. Ioannides, D.I. Kondarides, Chem. Eng. J. 134 (2007) 16–22.
[38] K.G. Azzam, I.V. Babich, K. Seshan, L. Lefferts, Appl. Catal. A: Gen. 338 (2008) 66–71.
[39] B.D. Morreale, M.V. Ciocco, R.M. Enick, B.I. Morsi, B.H. Howard, A.V. Cugini, K.S. Rothenberger, J. Membr. Sci. 212 (2003) 87–97.
[40] J.P. Collins, J.D. Way, Ind. Eng. Chem. Res. 12 (1993) 3006–3013.
[41] S. Tosti, M. Fabbricino, A. Moriani, G. Agatiello, C. Scudieri, F. Borgognoni, A. Santucci, J. Membr. Sci. 377 (2011) 65–74.
[42] P. Pinacci, M. Broglia, C. Valli, G. Capannelli, A. Comite, Catal. Today 156 (2010) 165–172.
[43] B.M. Faroldi, E.A. Lombardo, L.M. Cornaglia, Appl. Catal. A: Gen. 369 (2009) 15–26.